Exolith Lunar Simulants Constituent Report

exolithlab@ucf.edu

December 2023

Table of Contents

1 Context

Our goal is to develop and produce high-fidelity mineralogical simulants for the Moon, Mars, and asteroids. While one could make a chemically similar simulant for well-characterized planetary regolith using laboratory grade oxides, such a simulant would poorly reproduce many important regolith properties, including geotechnical properties. Mineralogy is the primary driver of these properties so we aim to simulate mineralogy in the correct proportions. Inevitably, naturally-occurring terrestrial minerals have experienced weathering and will contain at least small amounts of undesired mineral phases (contaminants). To control the quality of Exolith feedstock and identify reliable mineral sources with minimal contaminant phases, we verify the composition of each simulant constituent regularly.

The combination of X-ray fluorescence (XRF) and X-ray diffraction (XRD) techniques constrains mineral composition and can be used to identify the presence of contaminant phases. XRF analysis reveals the chemical composition of a sample. XRD analysis reveals crystal lattice spacing characteristic of particular mineral phases. The XRF and XRD data were acquired at the University of Central Florida's Materials Characterization Facility (MCF), with an exception for the basalt data as described in that section. All samples studied at the MCF were prepared as powders. The XRF data were acquired with a PANalytical Epsilon 1 XRF and concentrations of each compound were determined using Omnian software. The Epsilon 1 XRF uses a 50-kV silver X-ray tube. XRD data were acquired using a PANalytical Empyrean XRD Diffractometer. The Empyrean uses a 1.8-kW copper X-ray tube and a vertical goniometer with theta, theta geometry. We used HighScore software connected to the International Centre for Diffraction Data Powder Diffraction File to aid in XRD interpretation.

In 2021, reflectance spectra were obtained by Takahiro Hiroi at the Keck/NASA Reflectance Experiment Laboratory (RELAB; **http://www.planetary.brown.edu/relab/**). Visible-to-near-infrared spectra were obtained using a UV-Vis-NIR bidirectional reflectance spectrometer with an incidence angle of 30◦ and emergence angle of 0◦. Mid-infrared (thermal) spectra were obtained using a Thermo Nexus 870 FT-IR spectrometer.

Particle size analysis was conducted through a combination of sieve analysis and laser diffraction size analysis. Using a Gilson SS-14 Orbital Sieve Shaker, constituent minerals were analyzed down to 500 microns. A CILAS 1190 Laser Particle Size Analyzer was utilized at sizes less than 500 microns, and the two graphs (sieve and laser) were combined.

There have been 3 different batches of simulant constituents since the founding of the Exolith Lab, defined by the basalt source used:

Pebble Junction Basalt (Before 06/01/2021)

Butler Basalt (06/01/2021-07/31/2023)

Merriam Crater Basalt (08/01/2023-Present)

Batch numbers are provided on each simulant's website page, providing the appropriate spec sheet for each batch.

2 Simulant Constituent Analysis

2.1 Anorthosite

- Description: Igneous rock rich in plagioclase feldspar
- Source: Hudson Resources, Inc. GreenSpar
- Idealized Formula: $CaAl_2Si_2O_8$ (anorthite); $NaAl_2Si_2O_8$ (albite)

Notes Major phase anorthite confirmed by XRD analysis (Figure 2, Table 1). Presence of small quantities of albite also confirmed by XRD. The Hudson Resources website[1] reports that the GreenSpar anorthosite product is 90% plagioclase feldspar. Our XRF findings (Table 2) are consistent with those reported by Hudson and with the XRD results.

Figure 1. Photo of Greenspar Anorthosite

2.1.1 X-Ray Diffraction Pattern

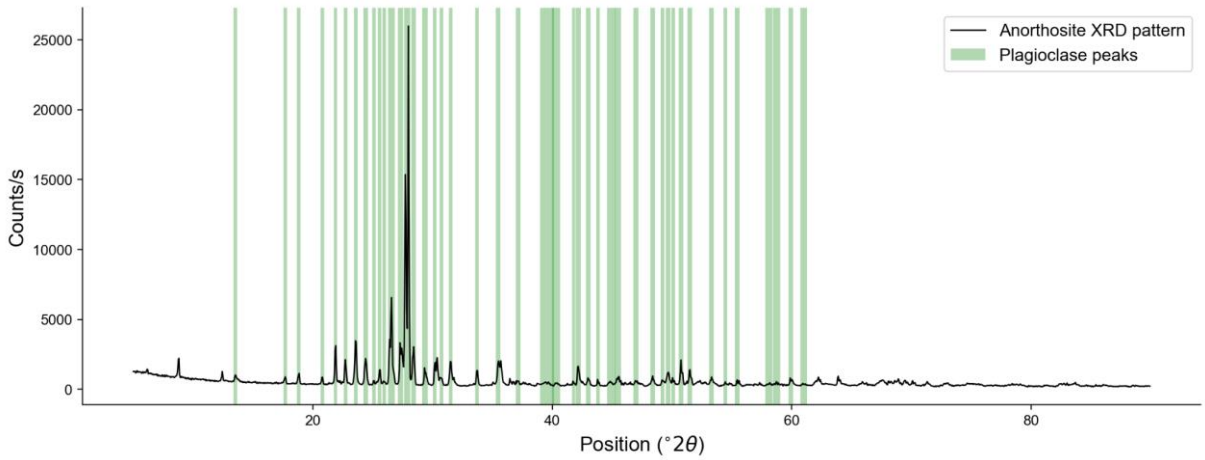

Figure 2: XRD pattern for anorthosite sample.

[1]https://hudsonresourcesinc.com/

Table 1. Anorthosite - XRD Pattern Peaks

Position (°2θ)	*Relative Intensity (%)*	*d-spacing (Å)*	*Matched By*
5.89	5.3	15.00	
8.80	10.0	10.05	
12.44	4.9	7.11	
13.55	4.1	6.53	Anorthite, albite
17.70	3.2	5.01	Anorthite
18.83	4.3	4.71	Anorthite, albite
20.79	3.5	4.27	Anorthite
21.90	15.1	4.06	Anorthite, albite
22.73	9.7	3.91	Anorthite, albite
23.59	17.6	3.77	Anorthite, albite
24.42	10.2	3.65	Anorthite, albite
25.10	2.2	3.55	Anorthite
25.60	6.2	3.48	Anorthite, albite
25.96	1.7	3.43	Anorthite, albite
26.57	31.9	3.35	Anorthite, albite
27.33	14.5	3.26	Anorthite
27.73	73.3	3.22	Anorthite, albite
28.01	100.0	3.19	Anorthite, albite
28.42	14.0	3.14	Anorthite, albite
29.37	5.6	3.04	Anorthite
30.19	8.2	2.96	Anorthite, albite
30.74	3.0	2.91	Anorthite, albite
31.51	9.1	2.84	Anorthite, albite
33.73	5.8	2.66	Anorthite, albite
35.49	8.9	2.53	Anorthite, albite
37.16	1.9	2.42	Anorthite, albite
39.56	1.2	2.28	Albite
40.31	1.1	2.24	Albite
41.78	1.5	2.16	Albite
42.17	7.4	2.14	Albite
43.02	2.7	2.10	Albite
43.83	1.9	2.07	Albite
44.90	1.5	2.02	Albite
45.49	2.8	1.99	Albite
46.99	1.9	1.93	Albite
48.39	3.5	1.88	Albite
49.19	2.3	1.85	Albite
49.68	5.1	1.84	Albite
50.11	1.9	1.82	Albite
50.76	7.8	1.80	Albite
51.49	6.0	1.77	Albite
53.31	3.1	1.72	Albite
54.45	1.4	1.69	Albite
55.46	2.1	1.66	Albite
58.08	0.9	1.59	Albite
58.72	1.2	1.57	Albite
59.91	2.6	1.54	Albite
60.99	0.8	1.52	Albite
62.22	3.4	1.49	
63.86	3.7	1.46	
65.83	1.2	1.42	
67.62	2.2	1.39	
68.89	2.5	1.36	
69.42	2.1	1.35	
70.06	1.9	1.34	
71.30	1.6	1.32	
72.91	1.1	1.30	
74.87	1.0	1.27	
78.44	0.7	1.22	
82.37	0.8	1.17	
83.65	1.1	1.16	
85.96	0.3	1.13	

Peak match citation: PDF 98-002-2022 (anorthite), PDF 98-000-9830 (albite) in Gates-Rector and Blanton (2019)

2.1.2 Chemistry from X-Ray Fluorescence

Table 2. Anorthosite - Bulk Chemistry

Compound	*Concentration (wt%)*
Al_2O_3	29.4
SiO_2	49.3
P_2O_5	1.0
SO_3	0.1
Cl	0.1
K_2O	0.3
CaO	19.0
TiO_2	0.1
Fe_2O_3	0.7
Total	100.0

2.1.3 FTIR Spectroscopy

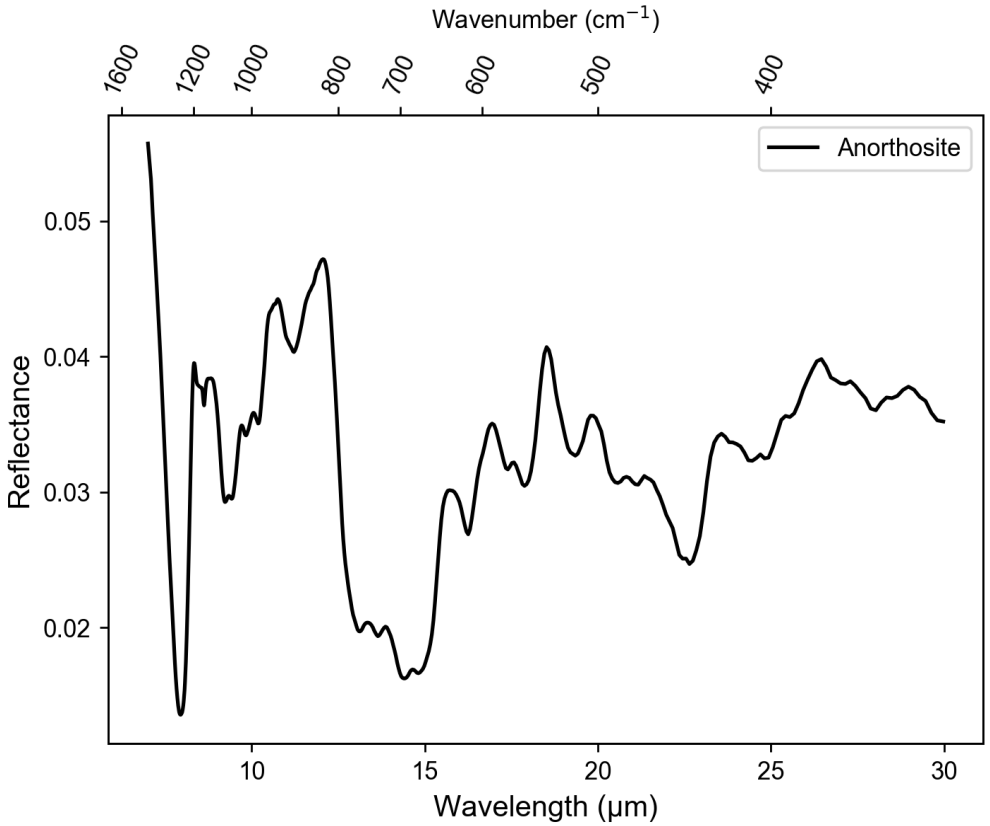

Figure 3. Anorthosite FTIR Spectroscopy

2.1.4 VIS NIR Spectroscopy

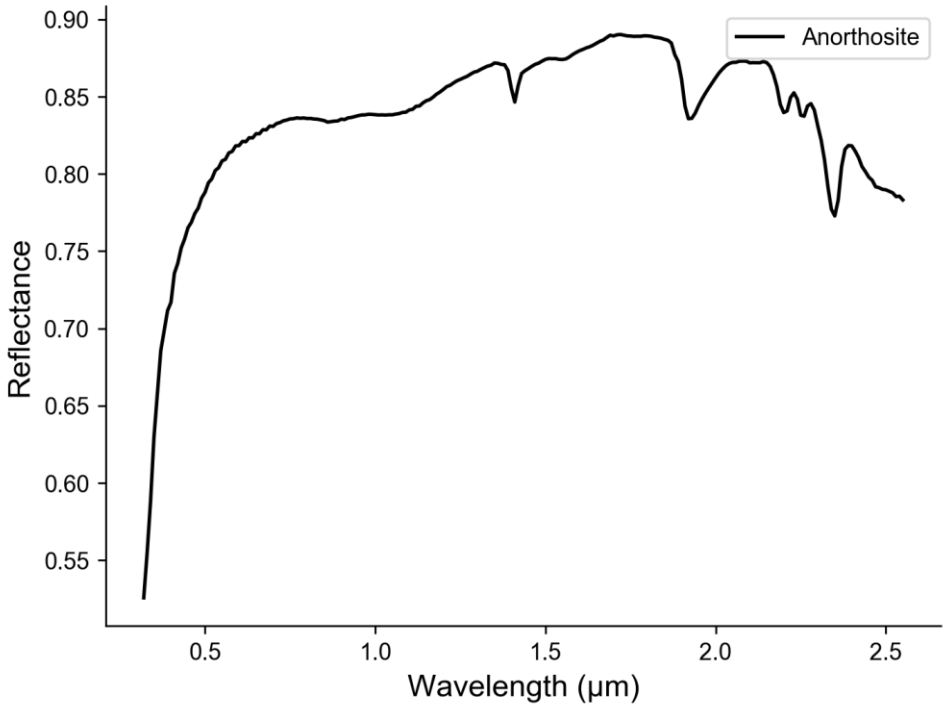

Figure 4. Anorthosite VIS NIR Spectroscopy

2.1.5 Anorthosite <250µm Particle Size Analysis

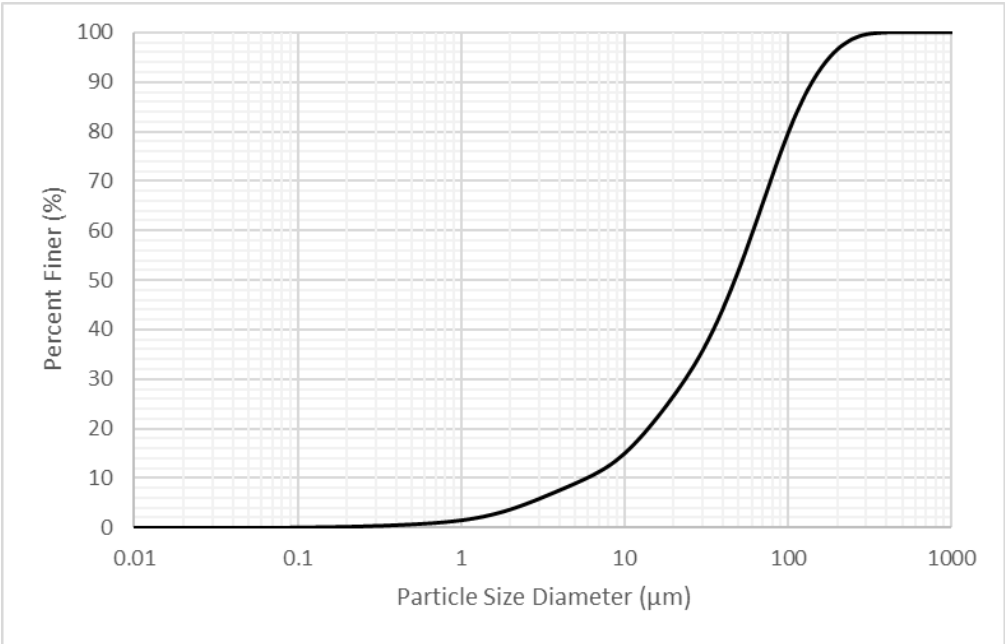

Figure 5. 250µm Anorthosite Particle Size Distribution

2.1.6 Anorthosite <2000µm Particle Size Analysis

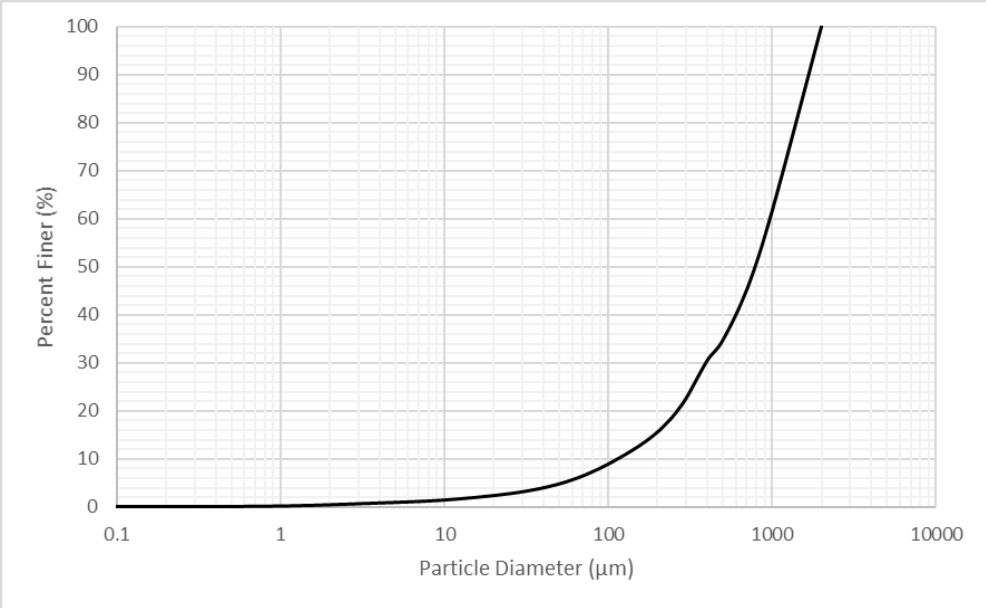

Figure 6. 2000µm Anorthosite Particle Size Distribution

2.2 Basalt (Merriam Crater)

Batch dates: 08/01/2023-Present

Description: Mafic igneous rock containing plagioclase, pyroxene, olivine, and volcanic glass

Source: Merriam Crater Basalt sourced from the Merriam Crater near Flagstaff, AZ. This is the same source as JSC-1A

Figure 7. Photo of Basalt.

2.2.1 Chemistry from X-Ray Fluorescence

Table 3. Basalt (Glass-Rich) - Approximate Bulk Chemistry

Compound	Concentration (wt %)
SiO_2	47.71
TiO_2	1.59
Al_2O_3	15.02
Fe_2O_3	10.79
MnO	0.19
MgO	9.39
CaO	9.9
Na_2O	2.7
K_2O	0.82
P_2O_5	0.66
Total	98.77

2.2.2 Basalt <1000µm Particle Size Analysis

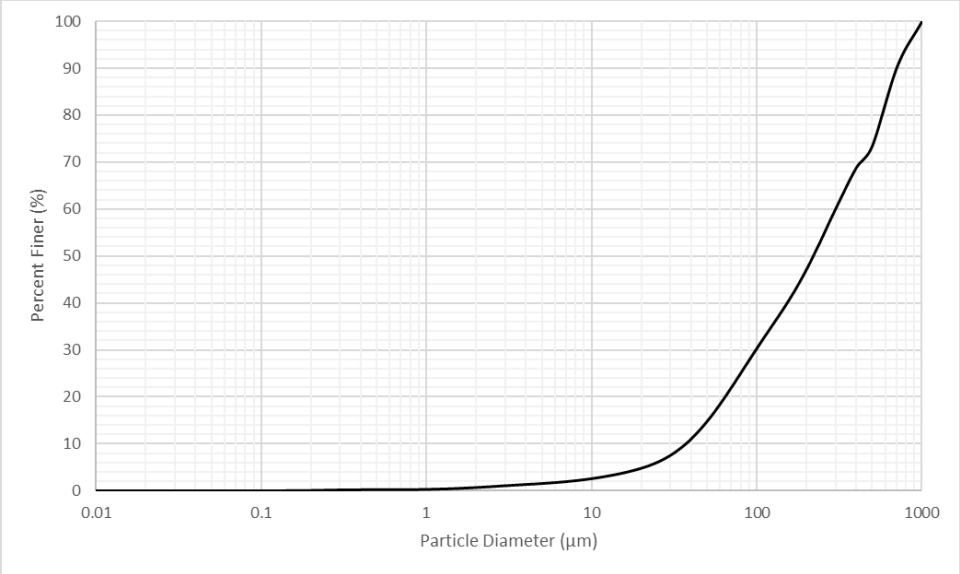

Figure 8. Basalt <1000µm Particle Size Distribution

2.2.3 Basalt <2000µm Particle Size Analysis

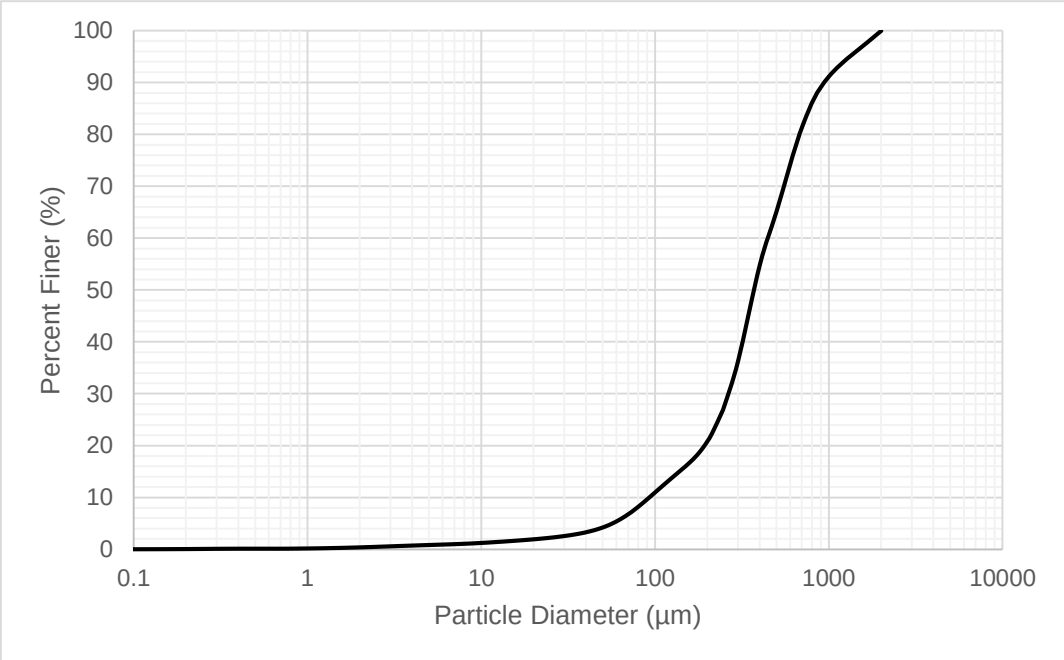

Figure 9. Basalt <2000µm Particle Size Distribution

2.3 Basalt (Butler)

Batch dates: 06/01/2021-07/31/2023

Description: Mafic igneous rock containing plagioclase, pyroxene, olivine, and volcanic glass

Source: Butler Arts Basalt

Figure 10. Photo of Basalt.

2.3.1 Chemistry from X-Ray Fluorescence

Table 4. Basalt (Glass-Rich) - Approximate Bulk Chemistry

Compound	Concentration (wt %)
SiO_2	45.7
TiO_2	2.5
Al_2O_3	15.5
Fe_2O_3	10.4
MnO	0.2
MgO	8.8
CaO	9.3
Na_2O	3.6
K_2O	2.1
P_2O_5	0.6
Total	98.7

2.3.2 Basalt <1000µm Particle Size Analysis

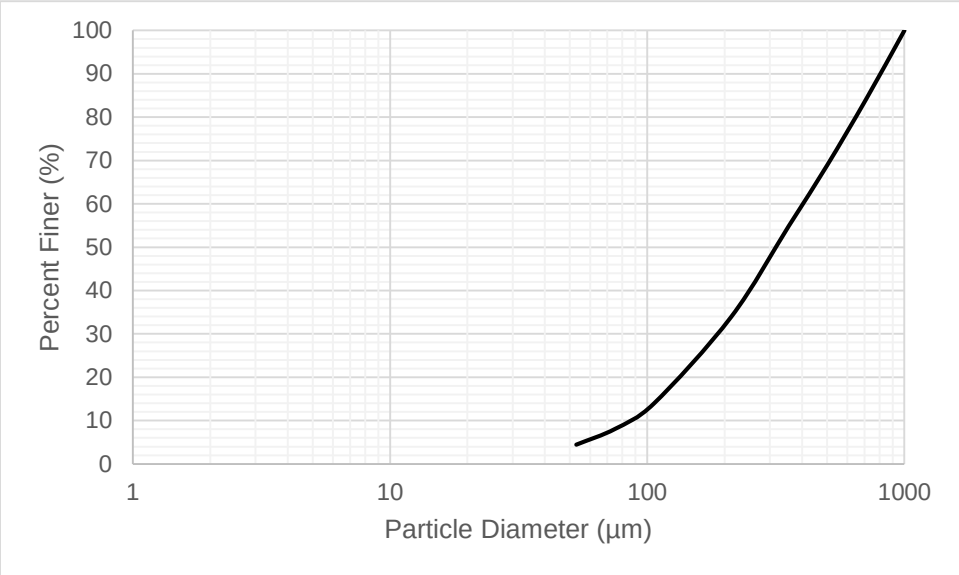

Figure 11. Basalt <1000µm Particle Size Distribution

2.4 Basalt (Pebble Junction)

Batch dates: Before 06/01/2021

Description: Mafic igneous rock containing plagioclase, pyroxene, olivine, and volcanic glass

Source: Pebble Junction

Figure 12. Photo of Basalt

2.4.1 Chemistry from X-Ray Fluorescence

Table 5. Basalt (Glass-Rich) - Approximate Bulk Chemistry

Compound	Concentration (wt %)
SiO_2	52.7
TiO_2	1.3
Al_2O_3	16.5
Fe_2O_3	9.1
MnO	0.1
MgO	5.8
CaO	8.2
Na_2O	3.8
K_2O	1.3
P_2O_5	0.4
Total	99.2

2.5 Bronzite

• Description: Pyroxene-group mineral

• Source: Stillwater Mine

• Idealized Formula: $(Mg,Fe)_3SiO_3$

Notes: Major phase confirmed by XRD analysis (Figure 14, Table 6). The XRF results (Table 7) are consistent with the expected composition of Bronzite.

Figure 13. Photo of Bronzite

2.5.1 X-Ray Diffraction Pattern

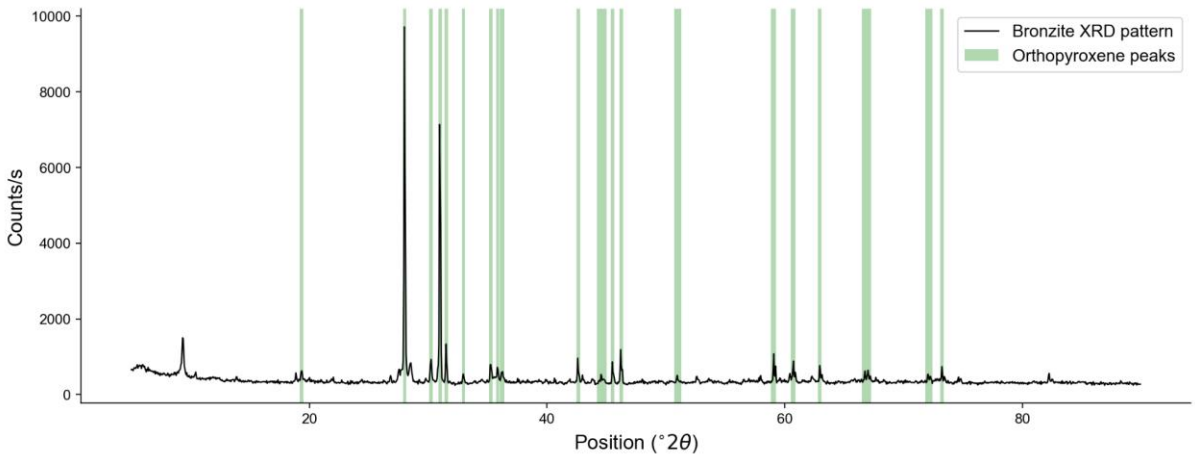

Figure 14. XRD Pattern for Bronzite Sample

Table 6. Bronzite - XRD Pattern Peaks

Position (°2θ)	*Relative Intensity (%)*	*d-spacing (Å)*	*Matched By*
5.77	5.0	15.31	
9.37	15.2	9.44	
19.35	4.1	4.59	Orthopyroxene $(Mg_{2.83}Fe_{1.17})Si_4O_{12}$)
28.02	100.0	3.18	Orthopyroxene $(Mg_{2.83}Fe_{1.17})Si_4O_{12}$)
28.52	7.2	3.13	
30.23	8.0	2.96	Orthopyroxene $(Mg_{2.83}Fe_{1.17})Si_4O_{12}$)
30.99	80.2	2.89	Orthopyroxene $(Mg_{2.83}Fe_{1.17})Si_4O_{12}$)
31.52	10.5	2.84	Orthopyroxene $(Mg_{2.83}Fe_{1.17})Si_4O_{12}$)
32.97	2.8	2.72	Orthopyroxene $(Mg_{2.83}Fe_{1.17})Si_4O_{12}$)
35.27	6.3	2.54	Orthopyroxene $(Mg_{2.83}Fe_{1.17})Si_4O_{12}$)
35.85	5.3	2.50	Orthopyroxene $(Mg_{2.83}Fe_{1.17})Si_4O_{12}$)
36.22	3.9	2.48	Orthopyroxene $(Mg_{2.83}Fe_{1.17})Si_4O_{12}$)
42.62	5.4	2.12	Orthopyroxene $(Mg_{2.83}Fe_{1.17})Si_4O_{12}$)
44.61	1.8	2.03	Orthopyroxene $(Mg_{2.83}Fe_{1.17})Si_4O_{12}$)
45.53	4.6	1.99	Orthopyroxene $(Mg_{2.83}Fe_{1.17})Si_4O_{12}$)
46.22	7.9	1.96	Orthopyroxene $(Mg_{2.83}Fe_{1.17})Si_4O_{12}$)
51.00	1.4	1.79	Orthopyroxene $(Mg_{2.83}Fe_{1.17})Si_4O_{12}$)
59.04	7.0	1.56	Orthopyroxene $(Mg_{2.83}Fe_{1.17})Si_4O_{12}$)
60.69	6.3	1.53	Orthopyroxene $(Mg_{2.83}Fe_{1.17})Si_4O_{12}$)
62.95	6.1	1.48	Orthopyroxene $(Mg_{2.83}Fe_{1.17})Si_4O_{12}$)
66.87	2.2	1.40	Orthopyroxene $(Mg_{2.83}Fe_{1.17})Si_4O_{12}$)
72.13	2.1	1.31	Orthopyroxene $(Mg_{2.83}Fe_{1.17})Si_4O_{12}$)
73.21	4.9	1.29	Orthopyroxene $(Mg_{2.83}Fe_{1.17})Si_4O_{12}$)
74.70	1.3	1.27	
82.22	3.6	1.17	

Peak match citation: PDF 98-018-8072 in Gates-Rector and Blanton (2019)

2.5.2 Chemistry from X-Ray Fluorescence

Table 7. Bronzite - Bulk Chemistry

Compound	*Concentration (wt%)*
MgO	27.5
Al_2O_3	3.3
SiO_2	45.0
P_2O_5	1.1
SO_3	0.1
Cl	0.2
K_2O	0.1
CaO	4.8
TiO_2	0.3
Cr_2O_3	0.7
MnO	0.3
Fe_2O_3	16.5
NiO	0.1
Total	99.9

2.5.3 FTIR Spectroscopy

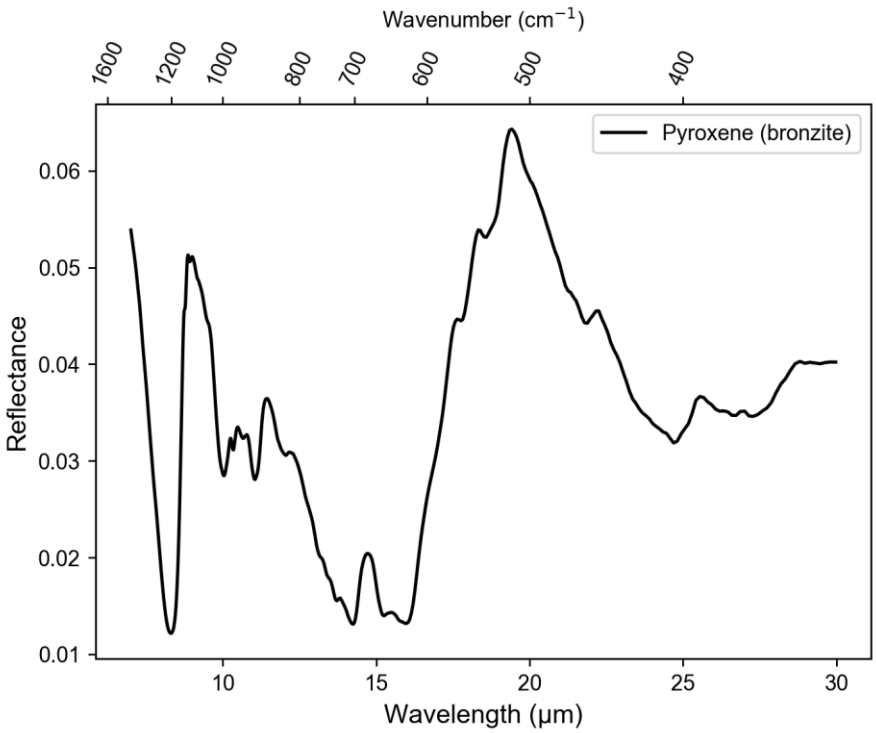

Figure 15. Bronzite FTIR Spectroscopy

2.5.4 VIS NIR Spectroscopy

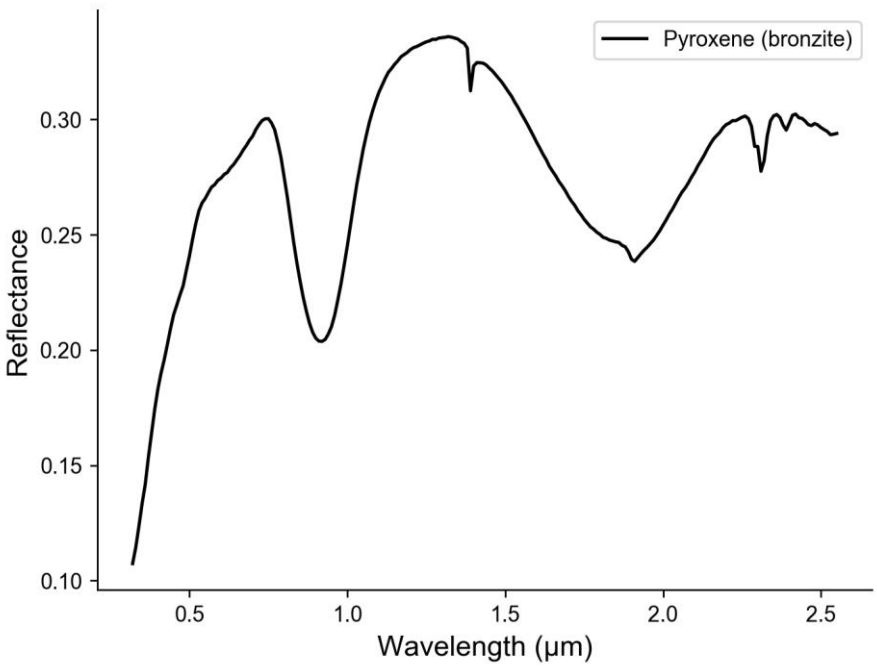

Figure 16. Bronzite VIS NIR Spectroscopy

2.5.5 Particle Size Analysis

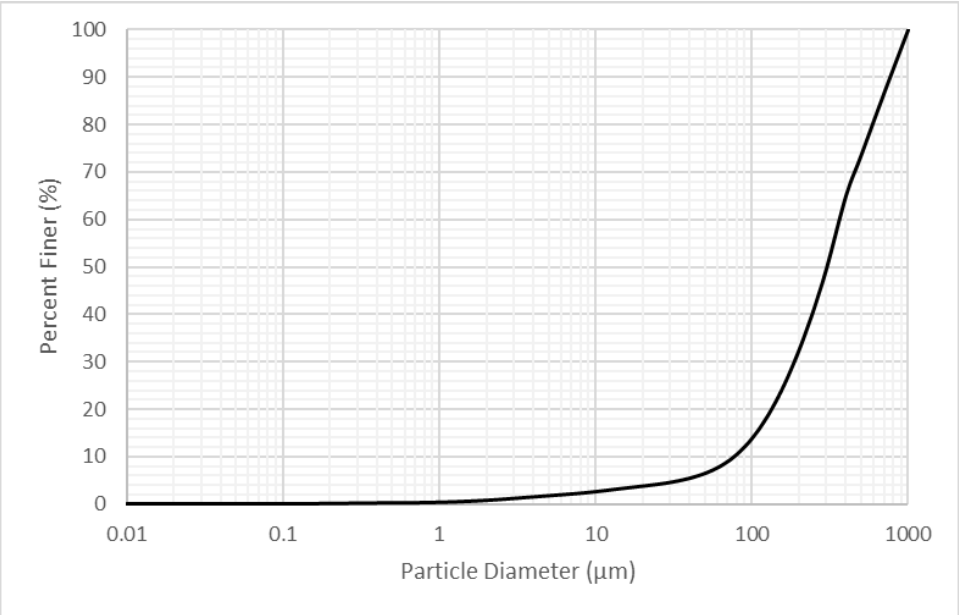

Figure 17. Bronzite Particle Size Distribution

2.6 Ilmenite

• Description: Titanium iron oxide

• Source: Ceramic Supply, Inc. Ilmenite – Powder

• Idealized Formula: $FeTiO_3$

• Also called: Manaccanite

Notes XRD analysis (Figure 19, Table 8) shows the presence of both ilmenite and titanium(IV) oxide. The most intense peak in the XRD diffractogram at $2\theta = 54.2^{\circ}$is associated with titanium(IV) oxide. XRF analysis (Table 9) shows concentration of 65.7 wt% TiO_2 and 26.9 wt% Fe_2O_3 with small amounts of MgO, Al_2O_3, and MnO.

Figure 18. Photo of Ilmenite

2.6.1 X-Ray Diffraction Pattern

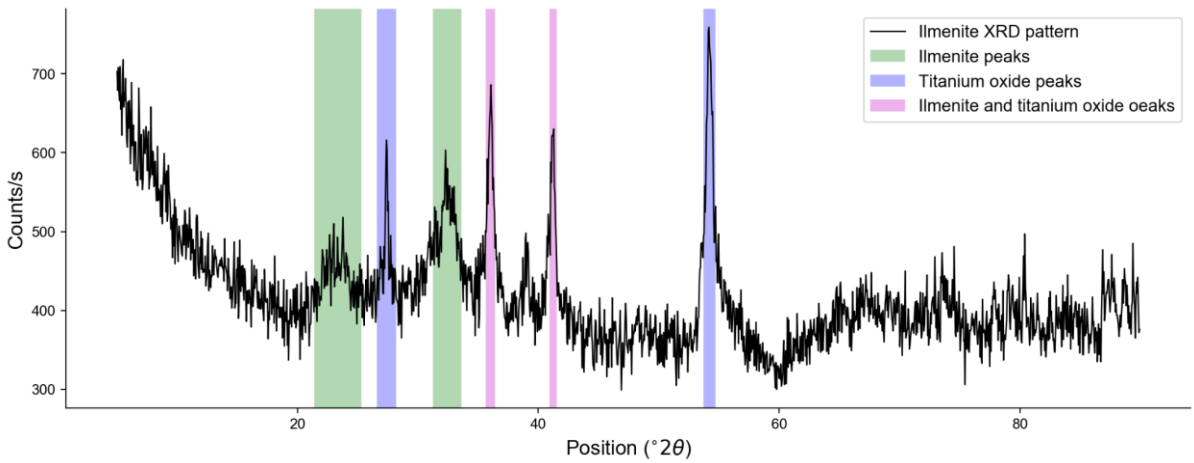

Figure 19. XRD Pattern for Ilmenite Sample

Table 8. Ilmenite - XRD Pattern Peaks

Position (°2θ)	*Relative Intensity (%)*	*d-spacing (Å)*	*Matched By*
23.35	17.9	3.81	Ilmenite
27.40	42.8	3.26	Titanium oxide
32.43	47.3	2.76	Ilmenite
36.03	75.7	2.49	Ilmenite, titanium oxide
41.23	67.1	2.19	Ilmenite, titanium oxide
54.21	100.0	1.69	Titanium oxide

Peak match citation: PDF 01-080-2530 and PDF 01-070-6267 in Gates-Rector and Blanton (2019)

2.6.2 Chemistry from X-Ray Fluorescence

Table 9. Ilmenite - Bulk Chemistry

Compound	*Concentration (wt%)*
MgO	2.7
Al_2O_3	1.7
SiO_2	0.4
P_2O_5	0.8
CaO	0.2
TiO_2	65.7
Cr_2O_3	0.1
MnO	1.2
Fe_2O_3	26.9
Nb_2O_5	0.1
Total	99.9

2.6.3 FTIR Spectroscopy

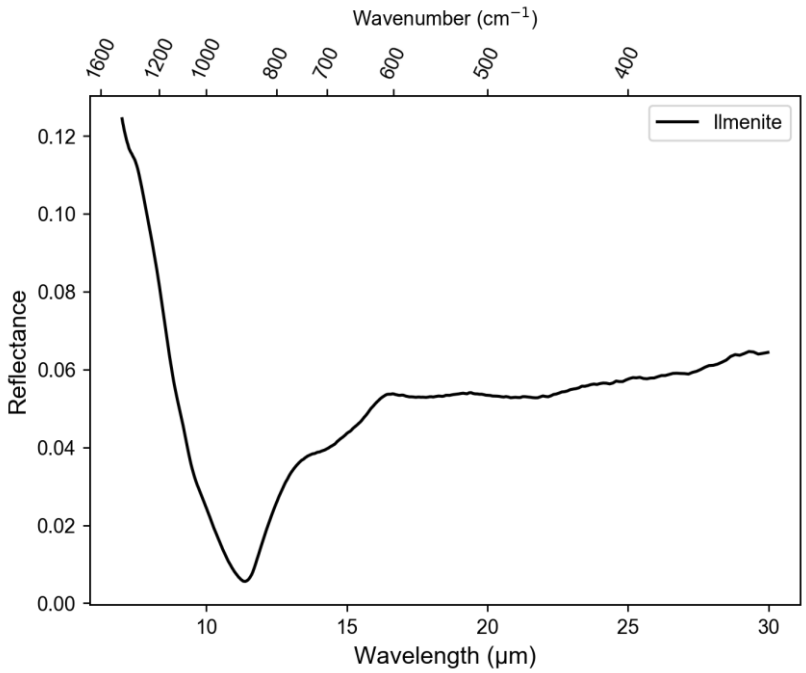

Figure 20. Ilmenite FTIR Spectroscopy

2.6.4 VIS NIR Spectroscopy

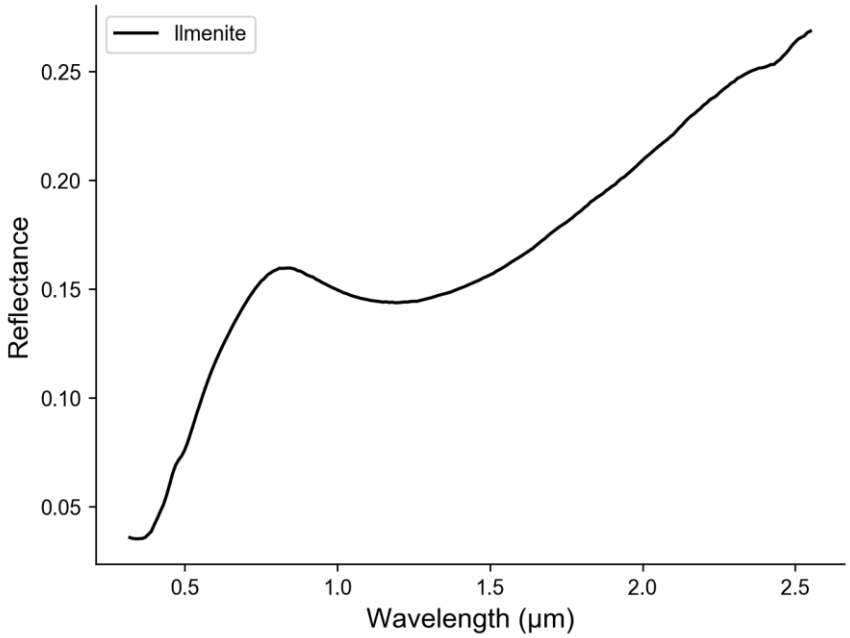

Figure 21. Ilmenite VIS NIR Spectroscopy

2.6.5 Particle Size Analysis

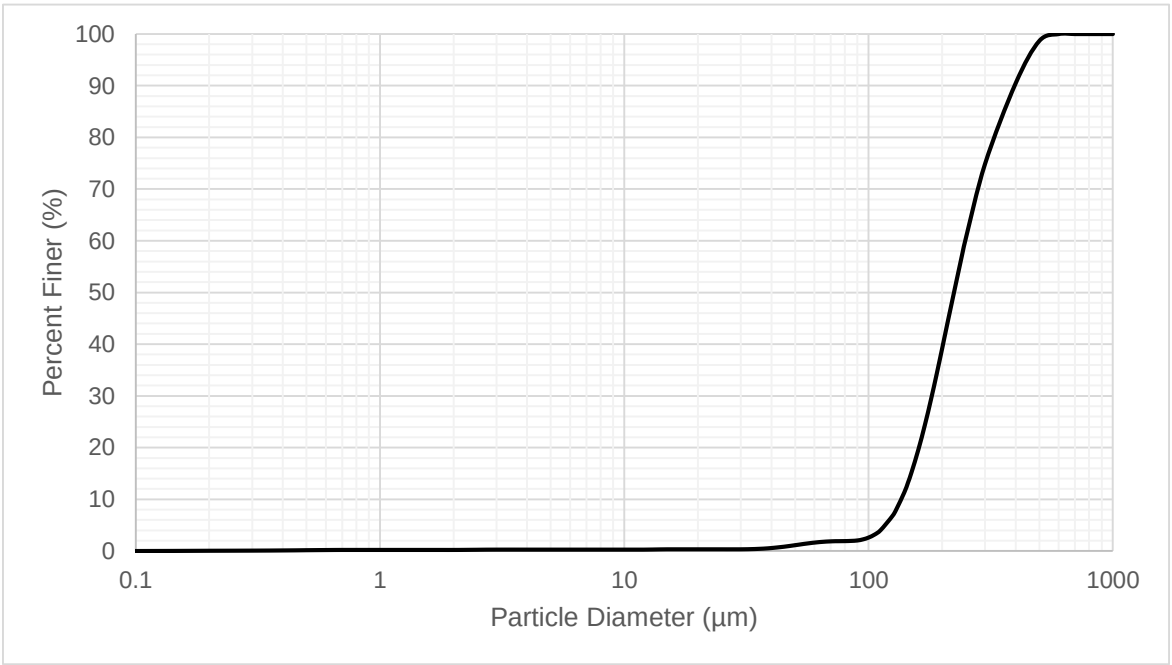

Figure 22. Ilmenite Particle Size Distribution

2.7 Olivine

• Description: Nesosilicate mineral

• Source: United Western Supply

• Idealized Formula: $(Mg, Fe)_2SiO_4$

Notes Major phase confirmed by XRD analysis (Table 10, Figure 24). XRF analysis (Table 11) is consistent with a high fraction of Mg-rich olivine (forsterite).

Figure 23. Photo of Olivine

2.7.1 X-Ray Diffraction Pattern

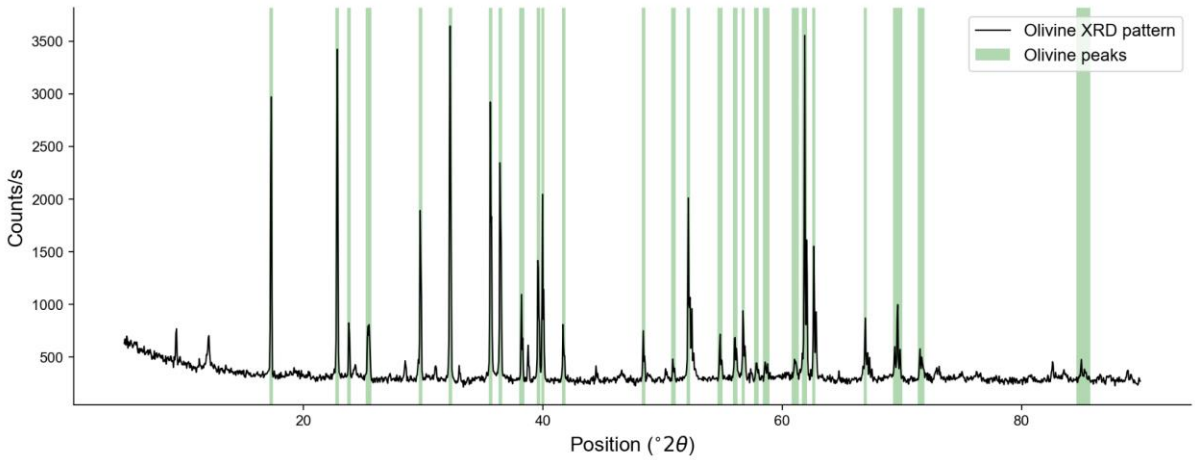

Figure 24. XRD pattern for Olivine sample

Table 10. Olivine - XRD Pattern Peaks

Position (°2θ)	*Relative Intensity (%)*	*d-spacing (Å)*	*Matched By*
9.37	9.6	9.44	
12.08	9.7	7.33	
17.30	74.2	5.13	Olivine $(Mg_{1.77}Fe_{0.23})SiO_4$
22.82	100.0	3.90	Olivine $(Mg_{1.77}Fe_{0.23})SiO_4$
23.82	15.6	3.74	Olivine $(Mg_{1.77}Fe_{0.23})SiO_4$
25.43	14.0	3.50	Olivine $(Mg_{1.77}Fe_{0.23})SiO_4$
28.50	5.5	3.13	
29.78	41.5	3.00	Olivine $(Mg_{1.77}Fe_{0.23})SiO_4$
32.26	91.6	2.77	Olivine $(Mg_{1.77}Fe_{0.23})SiO_4$
35.65	70.4	2.52	Olivine $(Mg_{1.77}Fe_{0.23})SiO_4$
36.46	53.6	2.46	Olivine $(Mg_{1.77}Fe_{0.23})SiO_4$
38.24	22.0	2.35	Olivine $(Mg_{1.77}Fe_{0.23})SiO_4$
39.63	33.7	2.27	Olivine $(Mg_{1.77}Fe_{0.23})SiO_4$
40.00	45.9	2.25	Olivine $(Mg_{1.77}Fe_{0.23})SiO_4$
41.73	11.3	2.16	Olivine $(Mg_{1.77}Fe_{0.23})SiO_4$
48.42	9.8	1.88	Olivine $(Mg_{1.77}Fe_{0.23})SiO_4$
50.91	4.0	1.79	Olivine $(Mg_{1.77}Fe_{0.23})SiO_4$
52.17	43.4	1.75	Olivine $(Mg_{1.77}Fe_{0.23})SiO_4$
54.80	11.8	1.68	Olivine $(Mg_{1.77}Fe_{0.23})SiO_4$
56.07	12.2	1.64	Olivine $(Mg_{1.77}Fe_{0.23})SiO_4$
56.74	20.1	1.62	Olivine $(Mg_{1.77}Fe_{0.23})SiO_4$
57.84	5.5	1.59	Olivine $(Mg_{1.77}Fe_{0.23})SiO_4$
58.66	3.9	1.57	Olivine $(Mg_{1.77}Fe_{0.23})SiO_4$
61.08	5.8	1.52	Olivine $(Mg_{1.77}Fe_{0.23})SiO_4$
61.86	73.0	1.50	Olivine $(Mg_{1.77}Fe_{0.23})SiO_4$
62.63	39.5	1.48	Olivine $(Mg_{1.77}Fe_{0.23})SiO_4$
66.93	16.7	1.40	Olivine $(Mg_{1.77}Fe_{0.23})SiO_4$
69.65	14.9	1.35	Olivine $(Mg_{1.77}Fe_{0.23})SiO_4$
71.60	5.4	1.32	Olivine $(Mg_{1.77}Fe_{0.23})SiO_4$
85.15	2.3	1.14	Olivine $(Mg_{1.77}Fe_{0.23})SiO_4$

Peak match citation: PDF 01-075-6789 in Gates-Rector and Blanton (2019)

2.7.2 Chemistry from X-Ray Fluorescence

Table 11. Olivine - Bulk Chemistry

Compound	*Concentration (wt%)*
MgO	44.3
Al_2O_3	0.8
SiO_2	39.6
P_2O_5	1.0
Cl	0.4
CaO	0.4
Cr_2O_3	0.5
MnO	0.2
Fe_2O_3	12.1
NiO	0.7
Total	100.0

2.7.3 FTIR Spectroscopy

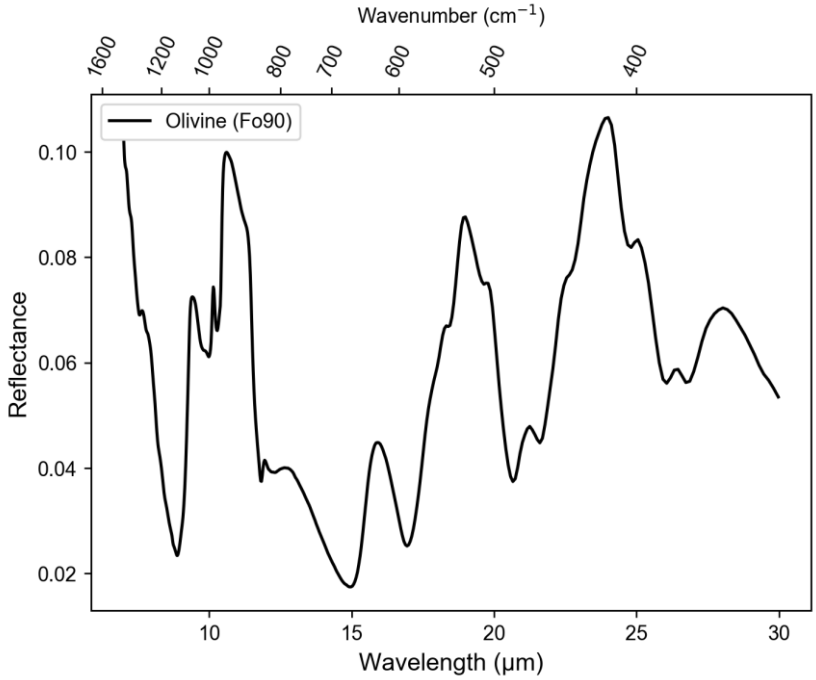

Figure 25. Olivine FTIR Spectroscopy

2.7.4 VIS NIR Spectroscopy

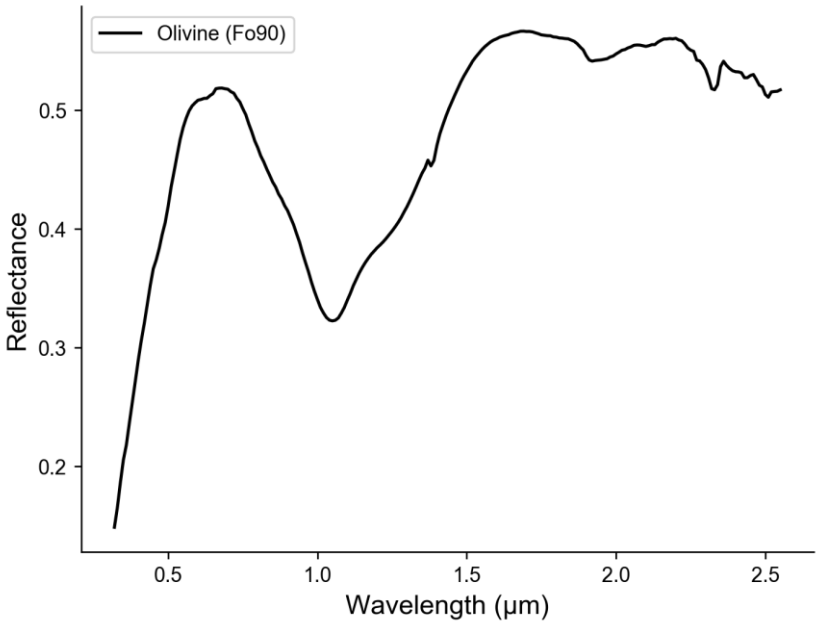

Figure 26. Olivine VIS NIR Spectroscopy

2.7.5 Particle Size Analysis

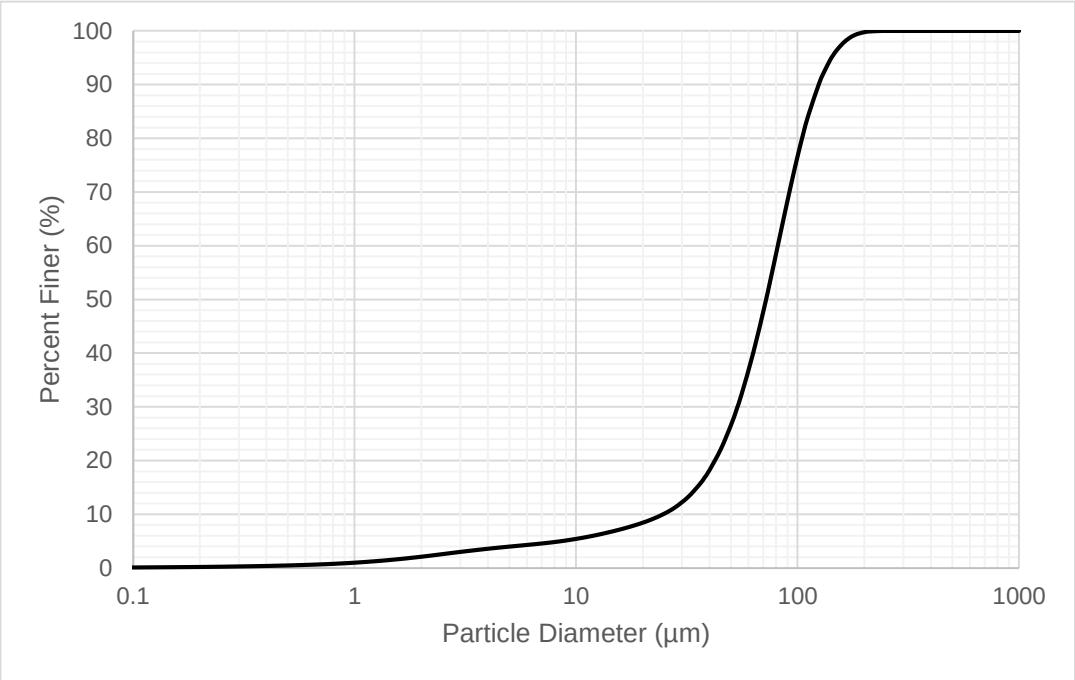

Figure 27. Olivine Particle Size Distribution

3 Acknowledgements

This work was supported by NASA Cooperative Agreement 80NSSC19M0214 to the Center for Lunar and Asteroid Surface Science (CLASS) as part of the Solar System Exploration Research Virtual Institute (SSERVI). This work was also supported by the Florida Space Institute at the University of Central Florida. The Exolith Lab gratefully acknowledges Kirk Scammon for collecting the XRF and XRD data. We also gratefully acknowledge Jesse Colangelo and Luis Zea who provided us with fused disk XRF data for basalt, funded by the University of Colorado, Boulder's Research Innovation Office.

References

Gates-Rector, S. and T. Blanton (2019). The powder diffraction file: a quality materials characterization database. *Powder Diffraction 34*(4), 352–360.